Master of Engineering Sciences

Intelligent Systems Engineering (ISI)

Sorbonne University

Bio-Inspired Vision

Characterization of Optical Sensors

Students (Group A+B):

Edouard David
Massin Assoul
Jessy Azizi
Haitem Bensalah
Amir Wail Bouhedja
Tony Cao
Benjamin Dukatar
Mohamed Mammeri

Academic Year 2024–2025

1 Introduction

In this report, we study the spectral response and analyze the noise (especially temporal and spatial noise) of an image sensor of the CMOS or CCD type. The experiments are carried out using the Synergie software, along with all the required measurement equipment.

How to Identify a CMOS or CCD Sensor

CMOS sensors can be distinguished from CCD sensors by looking at their physical characteristics and construction:

- **CMOS sensor:**
  - CMOS sensors integrate analog and digital circuits directly on the pixel array, which makes their structure more complex and visually crowded.
  - Their compact design often includes electronic components located directly around the pixel matrix.
- **CCD sensor:**
  - CCD sensors have a cleaner structure because the associated circuits are located outside the pixel matrix.
  - Their surface can be reflective, often metallized, due to the specific materials used in their fabrication.
- **Market positioning:**
  - CCD sensors are mostly used in high-end cameras requiring superior image quality.
  - CMOS sensors are widely used in modern technologies due to their low cost and versatility.

How to Identify a Black-and-White Sensor vs. a Color Sensor

- **Black-and-white sensor:** Black-and-white CMOS and CCD sensors use an array of photodetectors to convert light into an electrical signal.
- **Color sensor:** Color CMOS and CCD sensors also use a photodetector array, but each photodetector captures only one color component (red, green, or blue) thanks to a Bayer filter placed on top of the pixel array. To prevent interference from near-infrared light, which could be detected by the photodetectors and degrade color fidelity, an infrared low-pass filter is generally added in front of the sensor lens.

2 Study of the Spectral Response of the Detector and the Camera

2.1 Calibrated Detector and Spectral Response

With the calibrated detector, we measure a current $I_1(\lambda)$ in amperes (A), and the spectral responsivity $R_{dc}(\lambda)$ is expressed in (A/W). We do the same for the voltage $V_1(\lambda)$ measured

in volts (V), with a responsivity expressed in (V/W). We use a silicon diode of type UDS100.

2.2 Measurements with the Test Bench

The illustrated test bench is designed to measure the response of a sensor under test to monochromatic light. The light source emits light that is directed toward a monochromator, which selects a specific wavelength before sending it to an integrating sphere. The integrating sphere diffuses the light uniformly across its internal surface, ensuring a homogeneous light output and a uniform intensity distribution in all directions. The sensor under test is placed at the output of the integrating sphere, and a calibrated detector is also used to measure the optical intensity emitted by the sphere.

To perform the measurement, we use the Synergie software to configure the bench for our experiment. We then run a scan by varying the wavelength from 400 nm to 900 nm in steps of 10 nm, while observing the results inside the integrating sphere (see Figure 1 and Appendix).

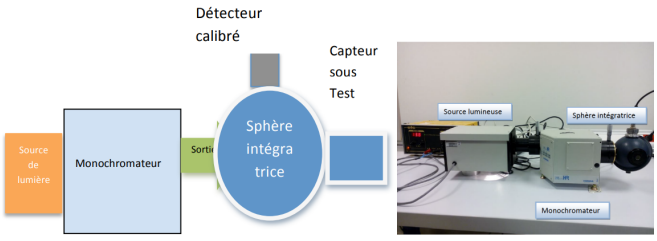

Figure 1: Diagram of the measurement bench.

2.3 Image Acquisition

Next, we position the sensor at the second output of the integrating sphere. Using *Pixel Cockpit*, we adjust the camera and observe the histogram. We observed second-order interference (see Figure 2), which allows us to detect wavelengths beyond 750 nm, i.e., in the near-infrared range, outside the visible spectrum.

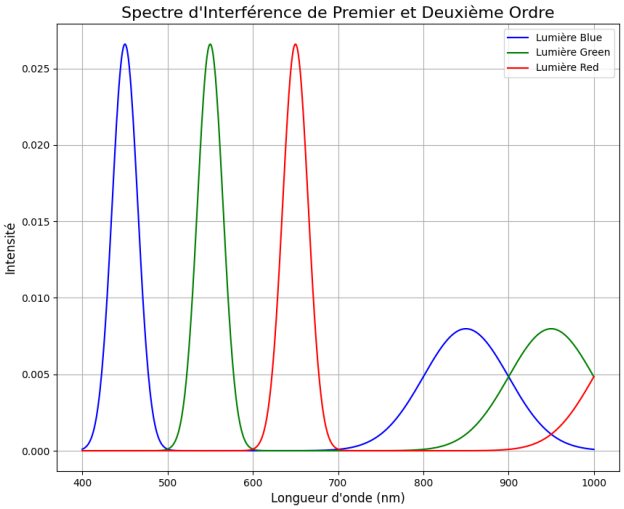

Figure 2: Interference spectrum: 1st and 2nd order for blue, green, and red light.

2.4 Exposure Time

We adjust wavelengths within the range [400 nm, 700 nm] and modify the parameters to avoid saturation. Using the histogram (see Figure 3), we tune the exposure time and the camera frame rate so that the peak is centered. The parameters are then saved into a `.ini` file. In our case, the response peak was around 590 nm.

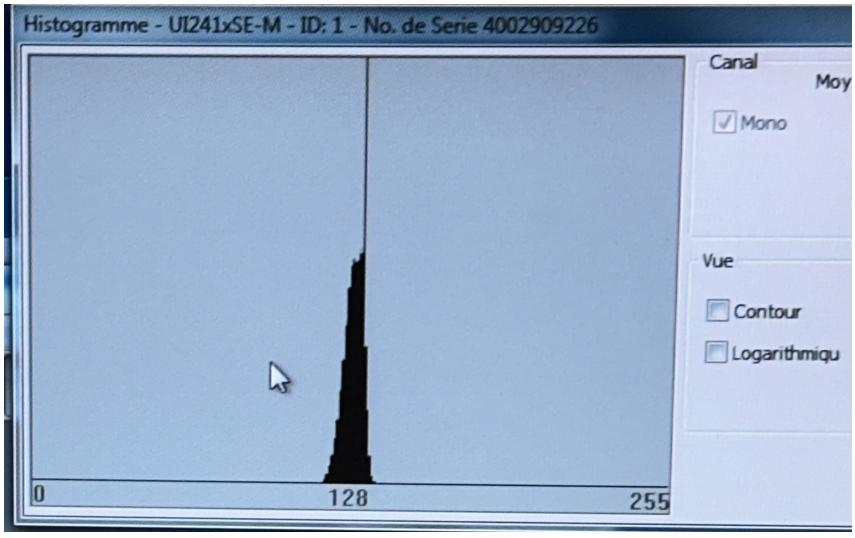

Figure 3: Typical image histogram.

2.5 Spectral Response Measurements

Once the camera and test-bench parameters are initialized, about 30 images are recorded for each wavelength in the interval [400 nm – 750 nm] with a 10 nm step. In addition, using the Synergie software, the current measured by the detector is recorded, which allows us to compute the optical power. These data, combined with the images, allow us to determine the spectral response of the camera.

First, using a first algorithm, we retrieve the current measurements to plot the optical power at the sphere output,

$$\Phi_{\text{output 1}}(\lambda) = \frac{I_1(\lambda)}{R_{\text{dc\_UDS100}}(\lambda)}$$

(see Figure 4).

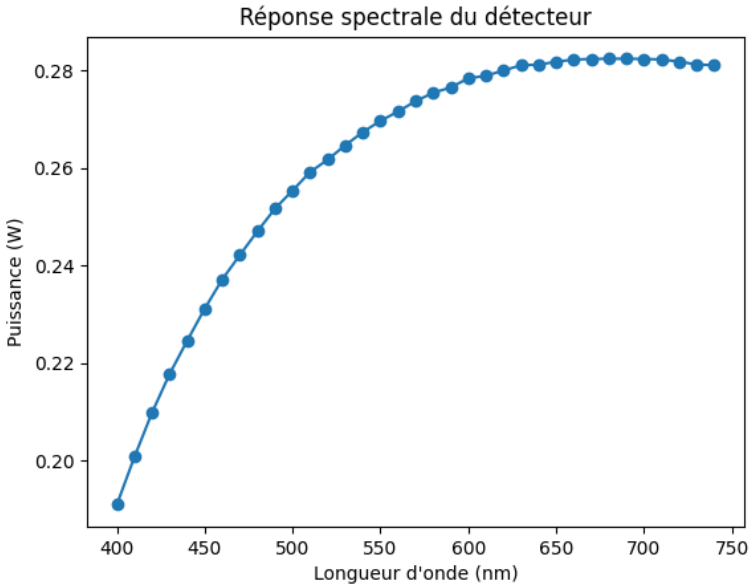

Figure 4: Optical power (calibrated detector) vs. wavelength.

We observe that the power first increases from 400 nm to 650 nm, then stabilizes around 700 nm.

Next, we compute the average of the images for each wavelength and display the camera spectral response as a function of wavelength (see Figure 5).

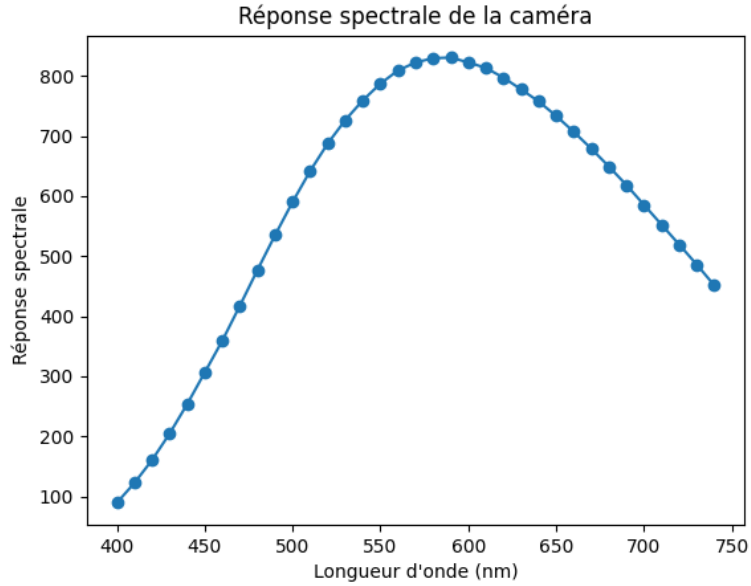

Figure 5: Camera response as a function of wavelength.

We observe that the camera shows a particularly strong response in the wavelength range between 550 nm and 600 nm, corresponding to green light. This increased sensitivity in this spectral band is typical of sensors optimized to efficiently capture visible light, especially in the region where the human eye is most sensitive.

Sensitivity decreases in the infrared regions due to physical limitations related to photon absorption in semiconductor materials. The decay also indicates that the camera is not designed to capture detailed information in the infrared.

3 Noise Study

In this part, we study the temporal and spatial noise of our camera using the test bench.

We adjust the entrance and exit slits of the monochromator as well as the camera exposure time as done previously. Then, we record around one hundred images at the integrating sphere input.

3.1 Mean Values and Noise

To visualize temporal noise, we plot the value of one pixel as a function of time to observe its evolution (see Figure 6).

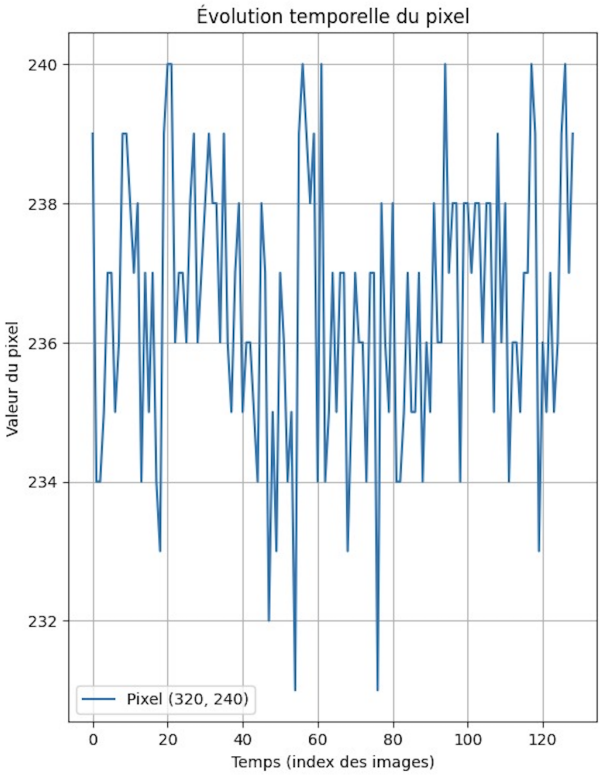

Figure 6: Pixel value over time (temporal noise).

The selected pixel value exhibits variations on the order of ± 10, which is a significant fluctuation. Although these variations may be due to electronic noise or other external factors, they are large enough to affect measurements. This highlights the importance of adjusting acquisition settings and averaging over multiple images to minimize the impact of these variations and obtain more reliable results.

To analyze spatial noise, we create a new image corresponding to the average of the 100 images (see Figure 7a). Then, we subtract this average image from a reference image in order to extract fixed-pattern spatial noise (see Figure 7b).

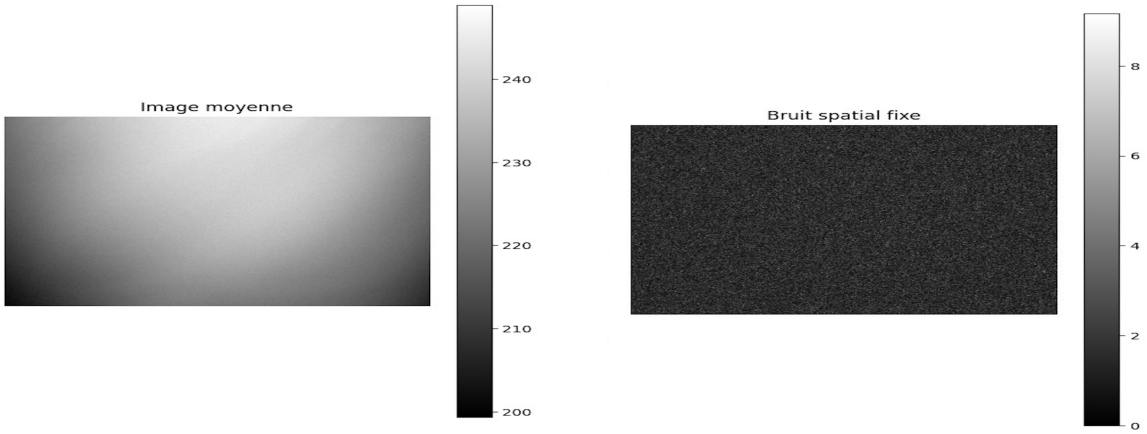

(a) Average image.

(b) Fixed-pattern spatial noise.

The image shows an average intensity computed for each pixel from 100 captured frames. We can see fixed patterns corresponding to so-called spatial noise. Spatial noise is due to differences in pixel sensitivity.

This method highlights noise variations that do not change over time, making it easier to analyze defects or irregularities that may be present in the images. By isolating this noise, we can better understand its characteristics and take measures to reduce or mitigate it in subsequent analyses.

Despite the presence of noise, it is possible to reconstruct a 3D image that reveals the shape of the sphere placed in front of the camera.

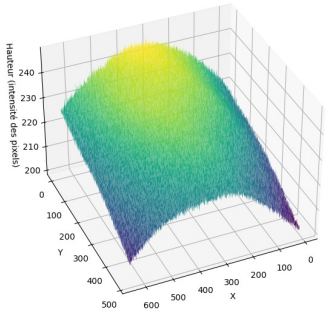

Figure 8: 3D average image.

4 Conclusion

Throughout this study, we analyzed the spectral response of an image sensor at different wavelengths using a dedicated test bench. We first measured the optical intensity through a monochromator, adjusting camera and detector parameters to minimize errors related to temporal and spatial noise. By processing the acquired images, we were able

to reduce noise using averaging and subtraction of reference images, enabling an accurate 3D reconstruction of the observed object.

This study demonstrates the importance of calibration and image processing in order to guarantee reliable and accurate measurements in optical detection systems.

Appendix: Wavelength Table and Observations

Wavelength (nm)	Observation
400	Violet
410	Light violet
420	Violet/Blue
430	Dark blue
440	Blue
450	Blue
460	Blue/Light blue
470	Cyan/Turquoise
480	Almost green
500	Green
510	Light green
520	Light yellow
530	Yellow
540	Dark yellow
550	Yellow/Orange
560	Light orange
570	Orange
580	Dark orange
590	Sunset orange
600	Orange
610	Light red
620	Red
630	Red
640	Flame red
650	Red/Burgundy
660	Red/Blue
670	Red/Blue
680	Almost blue
690	Dark pink
700	Dark pink
710	Pink toward violet
720	Pink toward violet
730	Pink toward violet
740	Violet
750	Violet (almost off)
760	Violet (almost off)
770	Violet (almost off)
780	Violet (almost off)
790	Violet (almost off)